Int. J. Solids Structures Vol. 29, No. 17, pp. 2201–2216, 1992
Printed in Great Britain.

0020–7683/92 $5.00 + .00
Pergamon Press Ltd

ANALYSIS OF PATCHED AND STIFFENED CRACKED PANELS USING THE BOUNDARY ELEMENT METHOD

A. YOUNG and D. P. ROOKE
Royal Aerospace Establishment, Farnborough, U.K.

and

D. J. CARTWRIGHT
Department of Mechanical Engineering, Bucknell University, Lewisburg, U.S.A.

(*Received* 22 *January* 1991; *in revised form* 29 *November* 1991)

Abstract—The Boundary Element Method is combined with the method of compatible deformations to analyse the stress distributions in cracked finite sheets symmetrically reinforced by bonded patches and stiffeners. The two-dimensional theoretical model involves an exact representation of the crack tip stress singularities and the stress intensity factors may be calculated directly. Examples of configurations are studied in order to demonstrate the practical use of the method, and it is shown that converged results from the model are representative of adhesively bonded structures.

1. INTRODUCTION

Cracks in aerospace structures tend to occur in regions of stress concentration, e.g. near edges, cutouts or fasteners. Therefore, the design and assessment of patch repairs to structural configurations must include the combined effects of the patch and nearby boundaries. The presence of nearby boundaries usually increases the rate of crack growth and hence reduces the fatigue life. Ignoring the effects of boundaries could lead to unsafe predictions of service lifetimes. Aircraft design often incorporates stiffeners to reinforce the strength of the thin sheet metal which comprises the fuselage and wings. It is therefore also desirable to include the influence of stiffeners when theoretically analysing cracked panels if the results are to be applied to practical structural configurations.

In the present work, the Boundary Element Method is coupled with the method of compatible deformations (Dowrick *et al.*, 1980; Dowrick, 1987; Young *et al.*, 1984, 1988, 1989), in order to analyse patched and stiffened finite sheets. This technique provides an accurate and versatile means of analysing many configurations of a reinforced cracked sheet, although the present two-dimensional theory is restricted to cases where the cracked sheet and the patches are isotropic, linearly elastic and the entire structure does not bend out of plane. The reinforced sheet configuration is analysed for static loading and the stress solution obtained from the model includes the values of the stress intensity factors at the crack tips.

2. DEVELOPMENT OF NUMERICAL MODEL

When a repair patch or a number of stiffeners are bonded to a thin flat sheet, the deformation of the sheet under loading is resisted by the reinforcing members. The influence of reinforcements on a sheet can be considered as a distribution of forces over the regions of attachment, which for balanced configurations (i.e. those in which the structure remains plane after deformation) may be considered as body forces. In this case, the behaviour of the sheet may be described using the theory of generalized plane stress and the theoretical modelling of the reinforced structure is reduced to a two-dimensional problem in terms of the unknown attachment force distributions. The solution for the attachment forces is obtained from the condition that the deformations of the sheet, adhesive layers, patches

and stiffeners under the action of the external loading and the attachment reaction forces are mutually compatible.

Define a set of rectangular Cartesian coordinates x_1, x_2, x_3 and consider a flat isotropic sheet of thickness h, tensile modulus E and Poisson's ratio v with a boundary (or boundaries) described by the contour Γ in the $\mathbf{x} \equiv (x_1, x_2)$ plane. The contour Γ is directed such that the interior of the sheet is to its left-hand side. Tractions (i.e. forces per unit thickness, per unit arc length) $t_j(\mathbf{x})$, where $j = 1, 2$ corresponds to the directions of x_1, x_2, exist on the boundary Γ and the sheet is loaded internally with distributions of body force per unit area $F_j^A(\mathbf{x})$ over a region A and force per unit arc length $f_j^L(\mathbf{x})$ over a line (or lines) L. These loading conditions are accompanied by a displacement field $u_j(\mathbf{x})$ at points $\mathbf{x}$ on or within the boundary Γ. The variables t_j, u_j, F_j^A and f_j^L $(j = 1, 2)$ in this configuration satisfy the following integral equation based on Somigliana's identity (Leipholz, 1974),

$$c_{ji}(\mathbf{x}_0)u_i(\mathbf{x}_0) = \int_\Gamma \{U_{ji}(\mathbf{x}, \mathbf{x}_0)t_i(\mathbf{x}) - T_{ji}(\mathbf{x}, \mathbf{x}_0)u_i(\mathbf{x})\}\, \mathrm{d}s(\mathbf{x}) + \frac{1}{h}\int\int_A U_{ji}(\mathbf{x}, \mathbf{x}_0)F_i^A(\mathbf{x})\, \mathrm{d}x_1\, \mathrm{d}x_2 + \frac{1}{h}\int_L U_{ji}(\mathbf{x}, \mathbf{x}_0)f_i^L(\mathbf{x})\, \mathrm{d}s(\mathbf{x}), \quad (1)$$

where $\mathrm{d}s(\mathbf{x}) = \{(\mathrm{d}x_1)^2 + (\mathrm{d}x_2)^2\}^{1/2}$ is the differential of arc length and repeated suffixes are summed. The term $T_{ji}(\mathbf{x}, \mathbf{x}_0)$ represents the traction distribution $(i = 1, 2)$ applied over points $\mathbf{x}$ on the boundary Γ, which in conjunction with a unit concentrated force acting in the j-direction at the point $\mathbf{x}_0 = (x_{01}, x_{02})$ on or within Γ, will give rise to the displacement field $U_{ji}(\mathbf{x}, \mathbf{x}_0)$ identical to that for the same force in an infinite unbounded sheet of the same material. The coefficients $c_{ji}(\mathbf{x}_0)$ of the free term on the left hand side of eqn (1) represent the contribution due to the concentrated force itself. Expressions for the fundamental displacement solution $U_{ji}(\mathbf{x}, \mathbf{x}_0)$ and the corresponding traction distribution $T_{ji}(\mathbf{x}, \mathbf{x}_0)$ may be obtained from infinite sheet solutions [see for example Muskhelishvili (1963)]. The fundamental solution obtained for a concentrated force in an intact infinite sheet is known as the Kelvin solution (Banerjee and Butterfield, 1981). Alternatively, a fundamental solution derived by Erdogan (1962) for a concentrated force in an infinite cracked sheet may be used. If the finite sheet to be modelled has a crack at the same location as in the infinite sheet, then the conditions $T_{ji}(\mathbf{x}, \mathbf{x}_0) = 0 = t_i(\mathbf{x})$ on the crack locus cause the contribution to the boundary integral in eqn (1) from the crack itself to be identically zero. In this case, the crack need not be included as part of the boundary Γ and the solution to eqn (1) will implicitly include the presence of the crack, along with the associated singular stress field at each crack tip. The integral eqn (1) will be used to represent a cracked sheet, using the Erdogan fundamental solution, and a patch, using the Kelvin solution.

Consider the following reinforced sheet configuration. An isotropic sheet of thickness h^s, tensile modulus E^s and Poisson's ratio v^s contains a straight crack located at $\{-a \leqslant x_1 \leqslant a,\ x_2 = 0\}$ and has distributions of traction $t_j^s(\mathbf{x})$ and displacement $u_j^s(\mathbf{x})$ on its boundary Γ^s. A number of isotropic patches are bonded to the sheet. The mth patch $(m = 1, 2, \ldots, M)$ is of thickness h_m^p, tensile modulus E_m^p and Poisson's ratio v_m^p and has tractions $t_j^{pm}(\mathbf{x})$ and displacements $u_j^{pm}(\mathbf{x})$ on its boundary Γ_m^p. The sheet and the mth patch are bonded together over a region A_m by means of an adhesive layer of thickness h_m^a and shear modulus μ_m^a, which is assumed to act linearly in shear only. Any other stresses which may exist in the adhesive are assumed to have a negligible effect on the load transfer. Denoting the component σ_{j3} $(j = 1, 2)$ of stress in the adhesive by τ_j^{am}, the reaction between the sheet and the mth patch at points $\mathbf{x}$ in A_m is represented by distributions of body force per unit area given by

$$F_j^{sm}(\mathbf{x}) = -F_j^{pm}(\mathbf{x}) = \tau_j^{am}(\mathbf{x}), \quad (2)$$

where the superscripts pm denote terms identified with the mth patch.

The condition that the deformations of the sheet and patch over the region A are compatible with the shear deflection of the adhesive layer may be expressed as

$$[u_j^{pm}(\mathbf{x}') - u_j^{pm}(\mathbf{x}'') - \Theta_j^m(\mathbf{x}' - \mathbf{x}'')] - [u_j^s(\mathbf{x}') - u_j^s(\mathbf{x}'')] = \frac{h_m^a}{\mu_m^a}[\tau_j^{am}(\mathbf{x}') - \tau_j^{am}(\mathbf{x}'')], \tag{3}$$

for $j = 1, 2$ and where $\mathbf{x}'$ and $\mathbf{x}''$ are two distinct points in the attachment region A_m, and $\Theta^m(\mathbf{x}) = (-\vartheta^m x_2, \vartheta^m x_1)$ accounts for any difference in the rigid body rotations (ϑ^m) of the patch and the sheet.

In addition, a number of stiffeners are bonded to the sheet over the loci L_n ($n = 1, 2, \ldots, N^{st}$). Each stiffener exerts a line distribution of force per unit arc length $f_j^n(\mathbf{x})$ ($j = 1, 2$; $n = 1, 2, \ldots, N^{st}$) on the corresponding locus L_n in the sheet, and itself experiences an equal and opposite reaction force $-f_j^n(\mathbf{x})$ along its length. The material and structural parameters of the nth stiffener are given by: length ℓ_n^{st}; width w_n^{st} over which the bond is assumed to act; cross-sectional area B_n^{st}; second moment of cross-sectional area I_n^{st}; tensile modulus E_n^{st}; shear modulus G_n^{st}; transverse flexural rigidity $D_n^{st} = E_n^{st} I_n^{st}$. The condition that the displacements of the sheet $u_j^s(\mathbf{x})$ and the nth stiffener $u_j^n(\mathbf{x})$ are compatible with the shear deflection of the adhesive layer, of thickness h_n^b and shear modulus μ_n^b, is similar to eqn (3) and is given in terms of f_j^n, the interaction force per unit length, by

$$[u_j^n(\mathbf{x}') - u_j^n(\mathbf{x}'')] - [u_j^s(\mathbf{x}') - u_j^s(\mathbf{x}'')] = \frac{1}{w_n^{st}} \frac{h_n^b}{\mu_n^b}[f_j^n(\mathbf{x}') - f_j^n(\mathbf{x}'')], \tag{4}$$

where $\mathbf{x}'$ and $\mathbf{x}''$ are distinct points on the nth stiffener locus L_n. The quantity $f_j^n(\mathbf{x})/w_n^{st}$ in eqn (4) corresponds to the shear stress σ_{rz} in the adhesive layer and is analogous to $\tau_j^{am}(\mathbf{x})$ in eqns (2) and (3) for the patch. As for the patch attachment earlier, other adhesive stress components are assumed to have negligible effects.

Under the action of the boundary tractions $t_j^s(\mathbf{x})$, $\mathbf{x}$ on Γ^s, the patch reactions $F_j^m(\mathbf{x})$, $\mathbf{x}$ in A_m ($m = 1, 2, \ldots, M$), and the stiffener reactions $f_j^n(\mathbf{x})$, $\mathbf{x}$ on L_n ($n = 1, 2, \ldots, N^{st}$), the integral equation (1) for the sheet becomes

$$c_{ji}^s(\mathbf{x}_0)u_i^s(\mathbf{x}_0) = \int_{\Gamma^s} \{U_{ji}^s(\mathbf{x}, \mathbf{x}_0)t_i^s(\mathbf{x}) - T_{ji}^s(\mathbf{x}, \mathbf{x}_0)u_i^s(\mathbf{x})\}\, ds(\mathbf{x})$$
$$+ \frac{1}{h^s}\sum_{m=1}^{M}\int\int_{A_m} U_{ji}^s(\mathbf{x}, \mathbf{x}_0)\tau_i^{am}(\mathbf{x})\, dx_1\, dx_2 + \frac{1}{h^s}\sum_{n=1}^{N^{st}}\int_{L_n} U_{ji}^s(\mathbf{x}, \mathbf{x}_0)f_i^n(\mathbf{x})\, ds(\mathbf{x}), \tag{5}$$

where eqn (2) has been used and the superscript s on the fundamental solution terms denotes those associated with the sheet material and crack geometry. Similarly, eqn (1) for the mth patch reduces to

$$c_{ji}^{pm}(\mathbf{x}_0)u_i^{pm}(\mathbf{x}_0) = \int_{\Gamma_m^p} \{U_{ji}^{pm}(\mathbf{x}, \mathbf{x}_0)t_i^{pm}(\mathbf{x}) - T_{ji}^{pm}(\mathbf{x}, \mathbf{x}_0)u_i^{pm}(\mathbf{x})\}\, ds(\mathbf{x})$$
$$- \frac{1}{h_m^p}\int\int_{A_m} U_{ji}^{pm}(\mathbf{x}, \mathbf{x}_0)\tau_i^{am}(\mathbf{x})\, dx_1\, dx_2. \tag{6}$$

When the source point $\mathbf{x}_0$ is taken to lie in the attachment regions A_m ($m = 1, 2, \ldots, M$) or L_n ($n = 1, 2, \ldots, N^{st}$), eqns (5) and (6) with the free-term coefficient $c_{ji}(\mathbf{x}_0) = \delta_{ji}$ (Kronecker delta) provide the interior displacements used in the compatibility eqn (3) or (4). Then for points $\mathbf{x}'$ and $\mathbf{x}''$ in A_m, but not on Γ^s or Γ_m^p, eqns (3), (5) and (6) give

$$\int_{\Gamma_m^p} [\Delta U_{ji}^{pm} t_i^{pm}(\mathbf{x}) - \Delta T_{ji}^{pm} u_i^{pm}(\mathbf{x})]\, ds(\mathbf{x}) - \int_{\Gamma^s} [\Delta U_{ji}^{s} t_i^{s}(\mathbf{x}) - \Delta T_{ji}^{s} u_i^{s}(\mathbf{x})]\, ds(\mathbf{x})$$

$$= \frac{1}{h^s} \sum_{n=1}^{N^{st}} \int_{L_n} \Delta U_{ji}^{s} f_i^n(\mathbf{x})\, ds(\mathbf{x}) + \frac{1}{h_m^p} \iint_{A_m} \Delta U_{ji}^{pm} \tau_i^{am}(\mathbf{x})\, dx_1\, dx_2$$

$$+ \frac{1}{h^s} \sum_{k=1}^{M} \iint_{A_k} \Delta U_{ji}^{s} \tau_i^{ak}(\mathbf{x})\, dx_1\, dx_2 + \frac{h_m^a}{\mu_m^a} [\tau_j^{am}(\mathbf{x}') - \tau_j^{am}(\mathbf{x}'')] + \Theta_j^m(\mathbf{x}' - \mathbf{x}''). \quad (7)$$

where

$$\Delta U_{ji}^{\alpha} = U_{ji}^{\alpha}(\mathbf{x}, \mathbf{x}') - U_{ji}^{\alpha}(\mathbf{x}, \mathbf{x}'') \quad \text{and} \quad \Delta T_{ji}^{\alpha} = T_{ji}^{\alpha}(\mathbf{x}, \mathbf{x}') - T_{ji}^{\alpha}(\mathbf{x}, \mathbf{x}''), \quad (8)$$

with $\alpha = pm$ for the mth patch and $\alpha = s$ for the sheet. If any part of the boundaries Γ^s or Γ_m^p coincides with the edge of the attachment region A_m, the displacement boundary values are used directly for the appropriate terms in eqn (3).

The requirement that the forces acting on each patch are in equilibrium provides $3M$ further equations of the form:

$$\int_{\Gamma_m^p} t_j^{pm}(\mathbf{x})\, ds(\mathbf{x}) - \frac{1}{h_m^p} \iint_{A_m} \tau_j^{am}(\mathbf{x})\, dx_1\, dx_2 = 0,$$

$$\int_{\Gamma_m^p} \{x_1 t_2^{pm}(\mathbf{x}) - x_2 t_1^{pm}(\mathbf{x})\}\, ds(\mathbf{x}) - \frac{1}{h_m^p} \iint_{A_m} \{x_1 \tau_2^{am}(x) - x_2 \tau_1^{am}\}\, dx_1\, dx_2 = 0. \quad (9)$$

Similarly, combining eqns (4) and (5) gives the compatibility equation for points $\mathbf{x}'$ and $\mathbf{x}''$ on the nth stiffener locus

$$[u_j^n(\mathbf{x}') - u_j^n(\mathbf{x}'')] - \int_{\Gamma^s} [\Delta U_{ji}^{s} t_i^{s}(\mathbf{x}) - \Delta T_{ji}^{s} u_i^{s}(\mathbf{x})]\, ds(\mathbf{x}) = \frac{1}{h^s} \sum_{m=1}^{M} \iint_{A_m} \Delta U_{ji}^{s} \tau_i^{am}(\mathbf{x})\, dx_1\, dx_2$$

$$+ \frac{1}{h^s} \sum_{n=1}^{N^{st}} \int_{L_n} \Delta U_{ji}^{s} f_i^k(\mathbf{x})\, ds(\mathbf{x}) + \frac{h_n}{w_n^{st} \mu_n^b} [f_j^n(\mathbf{x}') - f_j^n(\mathbf{x}'')]. \quad (10)$$

The displacements u_j^n of the nth stiffener in the above equation are most easily expressed in terms of an arc length parameter y measured in the longitudinal direction from one end. For notational clarity, the superscripts st, n, m are omitted here since the stiffeners act independently. The relative displacements of a thin stiffener due to a body force distribution $-f_i(y)$ per unit length ($0 < y \leqslant \ell$) are given by

$$u_1(y) - u_1(0) = [v_1(y) - v_1(0)] \cos\varphi - [v_2(y) - v_2(0)] \sin\varphi$$
$$u_2(y) - u_2(0) = [v_1(y) - v_1(0)] \sin\varphi + [v_2(y) - v_2(0)] \cos\varphi \quad (11)$$

where φ is the angle of orientation of the stiffener with respect to the 2-direction, and the displacements v_1 and v_2 of the stiffener in its own transverse and longitudinal directions respectively of the form

$$v_1(y) - v_1(0) = \frac{1}{BG} \left\{ y T_1(0) + \int_0^y (y - \eta) f_1(\eta)\, d\eta \right\}$$

$$- \frac{1}{D} \left\{ \frac{1}{2} y^2 M(0) + \frac{1}{6} y^3 T_1(0) + \int_0^y \frac{1}{6} (y - \eta)^3 f_1(\eta)\, d\eta \right\} - y\beta_{21}(0)$$

and

$$v_2(y)-v_2(0)=\frac{1}{BE}\left\{yT_2(0)+\int_0^y (y-\eta)f_2(\eta)\,d\eta\right\}, \tag{12}$$

with $T_1(y)$, $T_2(y)$ and $M(y)$ representing the internal forces and moment acting over the stiffener cross-section. In terms of the stresses σ_{ij} acting within the stiffener at points $(x,y,z)=(x_1\cos\varphi-x_2\sin\varphi, x_1\sin\varphi+x_2\cos\varphi, x_3)$, they are given by

$$T_1(y)=\int\int_B \sigma_{12}(x,y,z)\,dx\,dz \quad T_2(y)=\int\int_B \sigma_{22}(x,y,z)\,dx\,dz$$

and

$$M(y)=\int\int_B (x-\hat{x})\sigma_{22}(x,y,z)\,dx\,dz \tag{13}$$

such that the state of stress in the stiffener approximates to the following form

$$\sigma_{11}(x,y,z)\approx 0;\quad \sigma_{22}(x,y,z)\approx T_2(y)/B+(x-\hat{x})M(y)/I;\quad \sigma_{12}(x,y,z)\approx T_1(y)/B; \tag{14}$$

with $\hat{x}$ denoting the x-coordinate of the neutral axis and $\beta_{21}(0)$ denoting the partial derivative $\partial v_2/\partial x$ evaluated at the end $y=0$ [analogous to the rotation term Θ^m in eqn (3)]. Because the reinforcement is balanced, the out-of-plane stresses σ_{13}, σ_{23}, σ_{33} in the stiffener will have a negligible effect on $v_1(y)$ and $v_2(y)$.

In addition, the conditions that the stiffener is in equilibrium under the action of the body forces $-f_i(y)$ and the end loads $T_1(0)$, $T_1(\ell)$, $T_2(0)$, $T_2(\ell)$ and $M(0)$, $M(\ell)$ are given by

$$\int_0^\ell f_2(y)\,dy=T_2(\ell)-T_2(0),\quad \int_0^\ell f_1(y)\,dy=T_1(\ell)-T_1(0)$$

and

$$\int_0^\ell (\ell-y)f_1(y)\,dy=M(\ell)-M(0)-\ell T_1(0). \tag{15}$$

The end loads in eqns (15) correspond to boundary conditions for the stiffener. Setting all six values to zero will represent a stiffener with free ends. Alternatively, the values may be chosen to specify a given state of stress or strain at the ends. The latter case will arise when a section of a much larger stiffened structure is to be modelled and it is required that the stiffener should deform together with the underlying section of sheet at the ends.

3. DISCRETIZATION OF EQUATIONS

For a given loading and constraint on the reinforced sheet configuration, it is possible to determine the complete solution for the tractions and displacements on the boundaries of the sheet and patch and the reaction force distributions due to the patch and the stiffeners. In order to use eqns (5)–(15), the problem is discretized so that the integral equations derived in Section 2 may be reduced to a set of simultaneous linear equations.

The boundary Γ of the sheet or a patch is subdivided into a number of quadratic isoparametric elements, each containing three nodes: one at each end and one at the centre of the element (Bannerjee and Butterfield, 1981), those at the ends being in common with neighbouring elements. Then, the boundary integrals in eqns (5), (6), (7), (9) and (10) reduce to linear combinations of the nodal values of traction and displacement. The coefficients of the nodal boundary values are in the form of integrals, which are evaluated

numerically by Gauss quadrature [see Abramowitz and Stegun (1972) and Anderson (1965)].

The integrals involving the stiffener forces $f_i^n(\mathbf{x})$ in eqns (5), (7) and (10) may be treated similarly to those involving the boundary tractions $t_j(\mathbf{x})$. The loci of the stiffener reinforcements are subdivided into quadratic isoparametric elements and the integrals occurring in the stiffener deformation equations (11), (12) and (15) similarly reduce to linear sums of the nodal values.

An attachment region A_m, over which the sheet and a patch are bonded together, is subdivided into a number of elemental areas, referred to as cells, and the distribution of adhesive stress $\tau_i^{am}(\mathbf{x})$ is described in terms of nodal values associated with the cells. Over each cell, the spatial coordinates x_i and the adhesive shear stresses τ_i^{am} are all assumed to vary quadratically with respect to parametric coordinates (γ_1, γ_2), with $-1 \leqslant \gamma_1 \leqslant +1$, $-1 \leqslant \gamma_2 \leqslant +1$.

Consequently, each cell contains nine nodal points $\mathbf{x}^q$ and adhesive stress values τ_i^q $(q = 1, 2, \ldots, 9;\ j = 1, 2)$, although individual nodal values of adhesive stress may be common to two or more cells. Then the integrals in eqns (5)–(10) reduce to sums of terms associated with each cell of the form

$$\int\int_{\text{Cell}} U_{ji}(\mathbf{x}, \mathbf{x}_0)\tau_i^a(\mathbf{x})\,\mathrm{d}x_1\,\mathrm{d}x_2 = \sum_{q=1}^{9} \tau_i^q I_{ji}^q(\mathbf{x}_0), \tag{16}$$

and

$$I_{ji}^q(\mathbf{x}_0) = \int_{-1}^{+1}\int_{-1}^{+1} U_{ji}(\mathbf{x}(\gamma_1, \gamma_2), \mathbf{x}_0) M^q(\gamma_1, \gamma_2) J(\gamma_1, \gamma_2)\,\mathrm{d}\gamma_1\,\mathrm{d}\gamma_2, \tag{17}$$

where $M^q(\gamma_1, \gamma_2)$ are quadratic Lagrange shape functions and $J(\gamma_1, \gamma_2)$ is the Jacobian of the transformation from coordinates (x_1, x_2) to (γ_1, γ_2). The integrals $I_{ji}^q(\mathbf{x}_0)$ are evaluated using Gaussian quadrature.

However, when the source point $\mathbf{x}_0$ lies within the cell, the term $U_{ji}(\mathbf{x}, \mathbf{x}_0)$ contains a logarithmic singularity (see Appendix) which will cause numerical errors if Gaussian quadrature is used directly. In this case, the integrand in eqn (17) may be made continuous at $\mathbf{x} = \mathbf{x}_0$ by subtracting a suitable logarithmic singular term, which itself may be treated separately. If $\mathbf{x}_0$ coincides with the nodal point $\mathbf{x}^r$ on the cell and with the point $(\gamma_{01}, \gamma_{02})$ in the local transformed space, then the integrands in eqn (17) are all continuous $(q = 1, 2, \ldots, 9)$ except when $q = r$ in which case (17) may be rewritten

$$\begin{aligned} I_{ji}^r(\mathbf{x}^r) = \int_{-1}^{+1}\int_{-1}^{+1} \{ & U_{ji}(\mathbf{x}(\gamma_1, \gamma_2), \mathbf{x}^r) M^r(\gamma_1, \gamma_2) J(\gamma_1, \gamma_2) \\ & - \lambda_{ji} \ln[(\gamma_1 - \gamma_{01})^2 + (\gamma_2 - \gamma_{02})^2] J(\gamma_{01}, \gamma_{02}) \}\,\mathrm{d}\gamma_1\,\mathrm{d}\gamma_2 \\ & + \lambda_{ji} J(\gamma_{01}, \gamma_{02}) \int_{-1}^{+1}\int_{-1}^{+1} \ln[(\gamma_1 - \gamma_{01})^2 + (\gamma_2 - \gamma_{02})^2]\,\mathrm{d}\gamma_1\,\mathrm{d}\gamma_2. \end{aligned} \tag{18}$$

For a suitable choice of the quantities λ_{ji} $(i, j = 1, 2)$, the integrand enclosed by $\{\ \}$ is continuous and its integral is evaluated by Gaussian quadrature. Then the second integral in eqn (18) may be evaluated analytically (see Appendix). By considering the form of the function $U_{ji}(\mathbf{x}, \mathbf{x}_0)$ given in the Appendix, λ_{ji} are given by

$$\lambda_{ji} = -\frac{1}{2}\left[\frac{(3-\nu)(1+\nu)}{4\pi E}\right]\delta_{ji}, \tag{19}$$

except when $\mathbf{x}_0 = \mathbf{x}^r$ is on the crack in which case

$$\lambda_{ji} = -\frac{1}{2}\left[\frac{2}{\pi E}\right]\delta_{ji}. \tag{20}$$

Having discretized the distributions of traction and displacement on the boundaries and the internal attachment force distributions, the integral equations reduce to a set of simultaneous linear equations in the nodal values of traction, displacement and body force. If the sheet boundary Γ^s incorporates N^s nodes, the M patch boundaries Γ_1^p to Γ_M^p incorporate N^p nodes, the N^{st} stiffener loci L_1–$L_{N^{st}}$ incorporate N^L nodes and the M patched regions A_1–A_M incorporate N^A nodes, then the simultaneous linear equations will involve $(2N^s+2N^p+2N^A+M2N^L+N^{st})$ unknowns comprising the following: two from t_1^s, t_2^s, u_1^s, u_2^s at each node on the sheet boundary Γ^s; two from t_1^p, t_2^p, u_1^p, u_2^p at each node on the patch boundaries Γ_1^p–Γ_M^p; the adhesive stress components τ_1^a, τ_2^a at each node in each attachment region A_1–A_M; one scalar rotation parameter ϑ^m for each patch; the attachment forces f_1^{st}, f_2^{st} at each node on the stiffener loci L_1–$\Gamma_{N^{st}}$; one end condition $\beta_{21}(0)$ for each stiffener. The required number of equations are generated as follows:

(i) Equation (5) gives $2N^s$ simultaneous linear equations by taking the source point $\mathbf{x}_0$ at each of the N^s nodes on Γ^s and the unit force in the fundamental solution to be in the $j = 1$ or $j = 2$ direction.

(ii) Equation (6) gives $2N^p$ simultaneous linear equations by taking the source point $\mathbf{x}_0$ at each of the N^p nodes on the patch boundaries Γ_1^p–Γ_m^p and the unit force in the fundamental solution to be in the $j = 1$ or $j = 2$ direction.

(iii) Equation (7) gives $2N^A-2M$ simultaneous linear equations by fixing the source point $\mathbf{x}''$ at one of the nodes in each adhesion region A_1–A_m and taking the other source point $\mathbf{x}'$ to be at each of the remaining nodes in the same region with $j = 1$ or $j = 2$.

(iv) Equations (9) give $3M$ simultaneous linear equations for force and moment equilibrium of each of the M patches.

(v) Equation (10) gives $2N^L-2N^{st}$ simultaneous linear equations by fixing the source point $\mathbf{x}''$ at one end ($y = 0$) of each stiffener $L_1-L_{N^{st}}$ in turn and taking the other source point $\mathbf{x}'$ to be at each of the remaining nodes in the corresponding stiffener locus with $j = 1$ or $j = 2$.

(vi) Equations (15) give $3N^{st}$ simultaneous linear equations for force and moment equilibrium of each of the N^{st} stiffeners.

4. EVALUATION OF INTERNAL STRESS AND STRESS INTENSITY FACTORS

Values of stress at points interior to the boundary of the sheet or a patch may be obtained once the complete solution for displacements and tractions on the boundary and distributions of attachment force have been determined. Using Hooke's law and the linear elastic strain–displacement definitions, components of stress σ_{jk} ($j, k = 1, 2$) may be expressed as linear combinations of the partial derivatives of displacement $\partial u_i/\partial x_{ok}$ evaluated at the internal point $\mathbf{x}_0$ [see for example Leipholz (1974)]

$$\sigma_{jk}(\mathbf{x}_0) = \frac{E}{1+\nu}\left[\frac{1}{2}\left\{\frac{\partial u_j(\mathbf{x}_0)}{\partial x_{ok}} + \frac{\partial u_k(\mathbf{x}_0)}{\partial x_{oj}}\right\} + \left(\frac{\nu}{1-\nu}\right)\frac{\partial u_m(\mathbf{x}_0)}{\partial x_{om}}\delta_{jk}\right]. \tag{21}$$

These derivatives are readily obtained from the general equation (1), and take the form of an integral formula given by the right-hand side of eqn (1) with the kernels $U_{ji}(\mathbf{x}, \mathbf{x}_0)$ and $T_{ji}(\mathbf{x}, \mathbf{x}_0)$ replaced by their derivatives, $G_{kji}(\mathbf{x}, \mathbf{x}_0)$ and $H_{kji}(\mathbf{x}, \mathbf{x}_0)$, with respect to the spatial coordinate x_{ok} ($i, j, k = 1, 2$):

$$\frac{\partial u_i(\mathbf{x}_0)}{\partial x_{ok}} = \int_\Gamma \{G_{kji}(\mathbf{x}, \mathbf{x}_0)t_i(\mathbf{x}) - H_{kji}(\mathbf{x}, \mathbf{x}_0)u_i(\mathbf{x})\}\,ds(\mathbf{x})$$

$$+ \frac{1}{h}\int\int_A G_{kji}(\mathbf{x}, \mathbf{x}_0)F_i^A(\mathbf{x})\,dx_1\,dx_2 + \frac{1}{h}\int_L G_{kji}(\mathbf{x}, \mathbf{x}_0)f_i^L(\mathbf{x})\,ds(\mathbf{x}), \tag{22}$$

where

$$G_{kji}(\mathbf{x}, \mathbf{x}_0) = \frac{\partial}{\partial x_{ok}} U_{ji}(\mathbf{x}, \mathbf{x}_0) \quad \text{and} \quad H_{kji}(\mathbf{x}, \mathbf{x}_0) = \frac{\partial}{\partial x_{ok}} T_{ji}(\mathbf{x}, \mathbf{x}_0).$$

When the cracked sheet fundamental solution is used, the stress is infinite at the tips of the crack. By taking a series expansion of the differentiated kernels about either crack tip $\mathbf{x}_0 = (\pm a, 0)$, the kernels $G_{kji}(\mathbf{x}, \mathbf{x}_0)$ and $H_{kji}(\mathbf{x}, \mathbf{x}_0)$ are seen to depend locally on the inverse square root of the distance from $\mathbf{x}_0$ to the tip (see Appendix). The stress intensity factors can be defined as

$$K_{\mathrm{I}} = \lim_{\substack{r \to 0 \\ \psi = 0}} \{\sqrt{2\pi r}\sigma_{11}(\mathbf{x}_0)\} = \lim_{\substack{r \to 0 \\ \psi = 0}} \{\sqrt{2\pi r}\sigma_{22}(\mathbf{x}_0)\} \quad \text{and} \quad K_{\mathrm{II}} = \lim_{\substack{r \to 0 \\ \psi = 0}} \{\sqrt{2\pi r}\sigma_{12}(\mathbf{x}_0)\}, \tag{23}$$

where r, ψ are polar coordinates centred at the crack tip, such that $\mathbf{x}_0 = (\pm a \pm r\cos\psi, r\sin\psi)$.

Kernel functions, G^*_{kji} and H^*_{kji}, for the stress intensity factors may be analytically extracted from the singular leading terms in the series expansions of G_{kji} and H_{kji} about the crack tip; that is

$$G^*_{kji}(\mathbf{x}, \pm a) = \lim_{\substack{r \to 0 \\ \psi = 0}} \{\sqrt{2\pi r} G_{kji}(\mathbf{x}, \mathbf{x}_0\} \quad \text{and} \quad H^*_{kji}(\mathbf{x}, \pm a) = \lim_{\substack{r \to 0 \\ \psi = 0}} \{\sqrt{2\pi r} H_{kji}(\mathbf{x}, \mathbf{x}_0\}. \tag{24}$$

From the same procedure as that used to obtain internal stresses from eqns (21) and (22), the stress intensity factors, given by eqn (23), can be obtained by replacing G_{kji} and H_{kji} by G^*_{kji} and H^*_{kji} in eqn (22). Thus, the stress intensity factors are calculated directly from the boundary and attachment force solution. The derivatives of displacement (22), used to give the stress components at a point in the sheet or the patch, may be calculated directly using the complete solution of tractions and displacements on the boundary and the internal force distributions. The integrals in eqn (22) are reduced to linear expressions in terms of the nodal values from the solution in the same way as was described in Section 3. Since the point $\mathbf{x}_0$ is always interior to the boundary Γ, the boundary integrals in eqn (22) require no special treatment and may be evaluated using Gaussian quadrature. Provided $\mathbf{x}_0$ does not lie on one of the stiffener loci, the same approach may be used to evaluate the integrals over L in eqn (22).

The area integrals in eqn (22) may be treated as in eqns (16) and (17), except in the case where $\mathbf{x}_0$ lies within one of the adhesion cells and the integrand $G_{kji}(\mathbf{x}, \mathbf{x}_0)$ is singular. This singular case may be simply overcome provided that $\mathbf{x}_0$ coincides with one of the nine nodes in the cell. In this case, a certain function is subtracted from the integrand, thereby cancelling the singularity and admitting evaluation by Gaussian quadrature. The subtracted function is then integrated separately and recombined to give the required term in integral (22). Details of the singularities occurring in the kernel $G_{kji}(\mathbf{x}, \mathbf{x}_0)$ are given in the Appendix, and are found to be of the form

$$G_{kji}(\mathbf{x}, \mathbf{x}_0) = \frac{1}{\rho}\Phi_{kji}(\varphi) + 0(1), \tag{25}$$

where ρ and φ are defined by $\mathbf{x} - \mathbf{x}_0 = (\rho\cos\varphi, \rho\sin\varphi)$. If the point $\mathbf{x}_0$ coincides with the nodal point $\mathbf{x}^r$, then the integrand is singular in the coefficients of τ^r_j only; the coefficients of the other eight nodal values have continuous integrands due to the vanishing of the shape functions $M^m(\gamma_1, \gamma_2)$ at $\mathbf{x}^r$ for $m = r$. The term in question is of the form

$$\tau^r_i \int\int_{\text{Cell}} M^r(\gamma_1, \gamma_2) G_{kji}(\mathbf{x}, \mathbf{x}_0)\, \mathrm{d}x_1\, \mathrm{d}x_2$$

$$= \tau^r_i \int\int_{\text{Cell}} \left\{ M^r(\gamma_1, \gamma_2) G_{kji}(\mathbf{x}, \mathbf{x}_0) - \frac{1}{\rho}\Phi_{kji}(\varphi) \right\} \mathrm{d}x_1\, \mathrm{d}x_2 + \tau^r_i \int_{\substack{\text{Cell} \\ \text{Edge}}} \rho(\varphi)\Phi_{kji}(\varphi)\, \mathrm{d}\varphi, \tag{26}$$

where the integrand enclosed by { } is continuous at $\mathbf{x} = \mathbf{x}_0$. The second integral around the edge of the cell is obtained by using $dx_1\,dx_2 \equiv \rho\,d\rho\,d\varphi$ and performing the integration with respect to the radial distance ρ. This integral is evaluated by Gaussian quadrature on each of the four smooth sections of the cell edge.

Evaluation of the stress intensity factors K_I and K_{II} from eqn (23) using kernels (24) in eqn (22) requires no special treatment.

5. ADDITIONAL CONSIDERATIONS

The system of equations described at the end of Section 4 is solved numerically in matrix form using a computer program. The functions to be integrated, the subdivision of the regions Γ^s, Γ^p_m, A_m $(m = 1, 2, \ldots, M)$ and L_n $(n = 1, 2, \ldots, N^{st})$ into elemental sections and the numerical integration method are coded into the program essentially as set out in Sections 2, 3 and 4 and in the Appendix. However, there are some practical aspects of using the present method which have not so far been mentioned and these are given below.

(a) When considering crack problems, nodes may not be positioned on the crack itself. The cracked sheet fundamental solution is discontinuous across the crack locus and any crack line nodes must lie a small distance to one side or the other.

(b) In some configurations, an adhesion region A_m and/or a stiffener locus L_n and/or either boundary Γ^s or Γ^p_m may overlap. On such an intersection, all nodes of Γ^s, Γ^p_m, L_n and A_m must coincide exactly. If this condition were not imposed, the integral equations (5), (6), (7) and (10) would involve integrands which are singular at non-nodal positions and which would require special treatment not considered in Section 4.

(c) When modelling configurations involving symmetry boundary conditions, the condition of antisymmetry must also be imposed on the adhesive stress distribution.

(d) Integrals involving the functions $T_{ji}(\mathbf{x}, \mathbf{x}_0)$ in eqns (1), (6), (7), (8), (10) and $H_{kji}(\mathbf{x}, \mathbf{x}_0)$ in eqns (24) and (26) may be handled more easily in terms of the functions $Y_{ji}(\mathbf{x}, \mathbf{x}_0)$ and $Z_{kji}(\mathbf{x}, \mathbf{x}_0)$ defined by

$$T_{ji}(\mathbf{x}, \mathbf{x}_0) \equiv \frac{d}{ds(\mathbf{x})} Y_{ji}(\mathbf{x}, \mathbf{x}_0) \quad \text{and} \quad H_{kji}(\mathbf{x}, \mathbf{x}_0) \equiv \frac{d}{ds(\mathbf{x})} Z_{kji}(\mathbf{x}, \mathbf{x}_0) \tag{27}$$

with

$$Z_{kji}(\mathbf{x}, \mathbf{x}_0) = \frac{\partial}{\partial x_{ok}} Y_{ji}(\mathbf{x}, \mathbf{x}_0). \tag{28}$$

A function $Z^*_{kji}(\mathbf{x}, \mathbf{x}_0)$ may be similarly defined from $H^*_{kji}(\mathbf{x}, \mathbf{x}_0)$ for the stress intensity factors in eqns (15) and (17).

Then, integration by parts gives

$$\int_\Gamma T_{ji}(\mathbf{x}, \mathbf{x}_0) u_i(\mathbf{x})\, ds(\mathbf{x}) = [Y_{ji}(\mathbf{x}, \mathbf{x}_0) u_i(\mathbf{x})]_\Gamma - \int_\Gamma Y_{ji}(\mathbf{x}, \mathbf{x}_0) \frac{du_i(x)}{d\gamma}\, d\gamma$$

$$\int_\Gamma H_{kji}(\mathbf{x}, \mathbf{x}_0) u_i(\mathbf{x})\, ds(\mathbf{x}) = [Z_{kji}(\mathbf{x}, \mathbf{x}_0) u_i(\mathbf{x})]_\Gamma - \int_\Gamma Z_{kji}(\mathbf{x}, \mathbf{x}_0) \frac{du_i(x)}{d\gamma}\, d\gamma, \tag{29}$$

where γ is a parameter which varies continuously along each element on the boundary Γ. Choosing γ to be the local parameter in the elemental isoparametric transform (for which $u_i(\mathbf{x})$ is quadratic in γ), the derivatives $du_i(x)/d\gamma$ in eqns (32) may be expressed in terms of the nodal displacements and the linear derivatives of the shape functions. In the two-dimensional theory of generalized plane stress (Muskhelishvili, 1963), the function $Y_{ji}(\mathbf{x}, \mathbf{x}_0)$ may be expressed in closed form, and represents the resultant force across an arc due to a given distribution of stress or traction. The forms of the functions $Y_{ji}(\mathbf{x}, \mathbf{x}_0)$ and $Z_{kji}(\mathbf{x}, \mathbf{x}_0)$

are simpler than the corresponding $T_{ji}(\mathbf{x}, \mathbf{x}_0)$ and $H_{kji}(\mathbf{x}, \mathbf{x}_0)$, and are less expensive to evaluate. Details of this are given in the Appendix, where it can be seen that $Y_{ji}(\mathbf{x}, \mathbf{x}_0)$ is of similar form to the displacement function $U_{ji}(\mathbf{x}, \mathbf{x}_0)$; it has the same log-type singularities and may be evaluated together with $U_{ji}(\mathbf{x}, \mathbf{x}_0)$ at little extra computational effort.

6. EXAMPLE RESULTS

Two reinforced sheet configurations are now considered using the Boundary Element model developed in Sections 2–5. The first case demonstrates that the resulting solutions are representative of the required physical system by comparing numerical solutions with the exact solution for an axisymmetric patching configuration. The second case considers the effect of a patch and a stiffener on an edge cracked panel, and demonstrates the convergence of the stress intensity factor as the numbers of elements and cells are increased.

6.1. *A circular patch bonded to a large intact sheet*

If the sheet is infinite in size and remotely loaded in hydrostatic tension $\sigma_{11} = \sigma_{22} = \sigma$, the entire configuration is axisymmetric and the attachment problem may be solved in closed form. The exact solution, given in Young (1988), is to be compared with results from the present model using the two element mesh geometries, (i) and (ii), shown in Fig. 1(a, b). The chosen configuration for analysis by the Boundary Element model is of an uncracked square sheet of side 200 mm (i.e. $-100\text{ mm} \leqslant x_1 \leqslant 100\text{ mm}$, $-100\text{ mm} \leqslant x_2 \leqslant 100$ mm) loaded with tractions $t_1^s = 0$, $t_2^s = \pm\sigma$ on $x_2 = \pm 100$ mm and $t_1^s = \pm\sigma$, $t_2^s = 0$ on $x_1 = \pm 100$ mm. The entire stress solution is linear in σ and so the value chosen is $\sigma = 1$ GPa. The sheet has thickness $h^s = 1.5$ mm, tensile modulus $E^s = 70$ GPa and Poisson's ratio $\nu^s = 0.3$. A circular patch of radius $R = 30$ mm with an unloaded boundary is bonded to the sheet over the region $\{(x_1)^2 + (x_2)^2 \leqslant R^2\}$ by means of an adhesive layer of thickness $h^a = 0.15$ mm and shear modulus $\mu^a = 0.6$ GPa. The patch is of the same material as the sheet with thickness $h^p = 1.5$ mm, tensile modulus $E^p = 70$ GPa and Poisson's ratio $\nu^p = 0.3$.

Two different meshes of elements and cells are used to study this problem, and are shown in Fig. 1. The first mesh (i), in which the entire structure is considered, involves the subdivision of $A\{(x_1)^2 + (x_2)^2 \leqslant R^2\}$ into five cells (with 25 nodes) with four elements on the patch boundary Γ^p. Each of the four edges of the sheet boundary Γ^s is subdivided into four equal elements. In this configuration, the boundary conditions consist of values of traction only and it is necessary to apply three nodal displacement boundary values to each

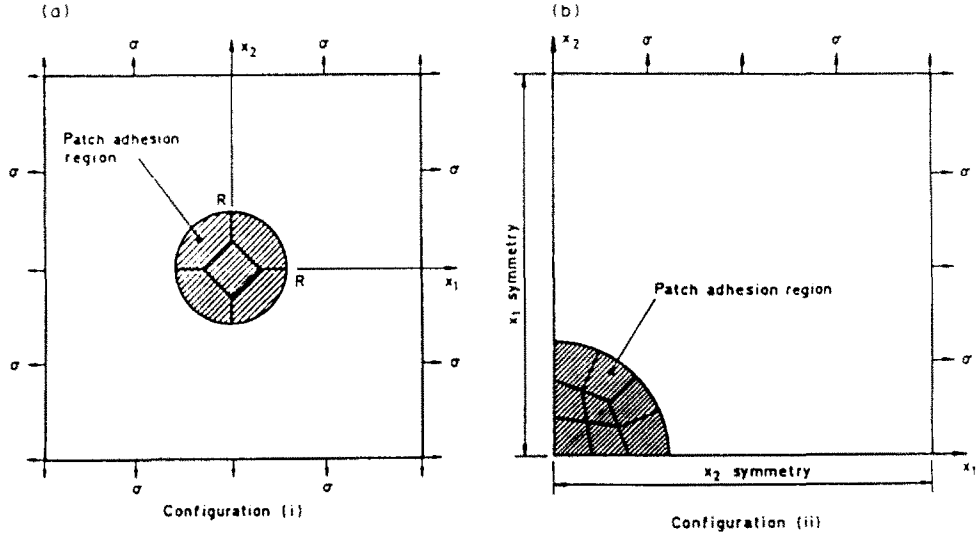

Fig. 1. Circular patch bonded to a large biaxially loaded sheet. (Example 1 showing the cell subdivision used in the two configurations (i) and (ii) analysed.)

of the sheet and patch in order to constrain the otherwise arbitrary rigid body translation and rotation. The second mesh (ii) exploits the symmetry of the problem about the x_1 and x_2 axes, and only one quadrant of the structure is considered ($x_1 \geqslant 0, x_2 \geqslant 0$) with boundary conditions $t_1 = 0 = u_2$ on $x_2 = 0$ and $t_2 = 0 = u_1$ on $x_1 = 0$. The attachment region $A^+\{(x_1)^2+(x_2)^2 \leqslant R^2, x_1 \geqslant 0, x_2 \geqslant 0\}$ is subdivided into eight cells (43 nodes) with 10 elements (20 nodes) on the patch boundary, and a total of 36 equal elements (72 nodes) are used on the sheet boundary. In accordance with consideration (c) in Section 5, antisymmetry conditions are also imposed on the adhesive stress, i.e. $\tau_2^a = 0$ on $x_2 = 0$ and $\tau_1^a = 0$ on $x_1 = 0$.

The results from the present model are compared with the exact axisymmetric solution for the radial component of adhesive shear stress $\tau_r^a = [(\tau_1^a)^2+(\tau_2^a)^2]^{1/2}$ in Fig. 2. The adhesive shear stress radial component is zero at the patch centre and attains its largest value at the patch edge. Both configurations give solutions which are consistent with the exact solution, with errors occurring at the patch edge, of 6% for subdivision (i) and 4% for subdivision (ii). The tractions on the boundaries $x_1 = 0$ and $x_2 = 0$ of the sheet and the patch in the symmetric case (ii) and values of stress calculated at the internal attachment cell node positions in case (i) also give agreement with the exact solution; the largest errors are 8% for subdivision (i) and 4% for subdivision (ii). The errors in the solution are seen to diminish when the mesh of cells and elements is refined, and it is concluded that the present model may be used to obtain accurate solutions for adhesively bonded reinforcements to thin sheets.

6.2. *A patch and a stiffener bonded to an edge-cracked sheet*

The configuration to be studied is schematically illustrated in Fig. 3, and the thicknesses and elastic properties of the sheet, patch and adhesive layer are as used in example (1) above. The sheet is rectangular of dimensions $0 \leqslant x_1 \leqslant 90$ mm, -90 mm $\leqslant x_2 \leqslant 90$ mm and contains an edge-crack located at $0 \leqslant x_1 \leqslant a$, $x_2 = 0$; two values of crack-length $a = 14.99$ and $a = 29.99$ are considered. The left-hand tip of the crack in the fundamental solution is located outside the boundary of the sheet and does not affect the solution. The sheet is loaded uniaxially with values of traction $t_2 = \pm\sigma$ on the edges $x_2 = \pm 90$ mm, all other tractions on Γ^1 and Γ^p being zero (as earlier, the value $\sigma = 1$ GPa is used).

A stiffener of length $\ell^{st} = 120$ mm parallel to the 2-direction is bonded to the sheet at position $x_1 = 15$ mm, -60 mm $\leqslant x_2 \leqslant 60$ mm. The material parameters of the stiffener and its adhesive layer are given by: cross-sectional area $B^{st} = 6$ mm^2, tensile modulus

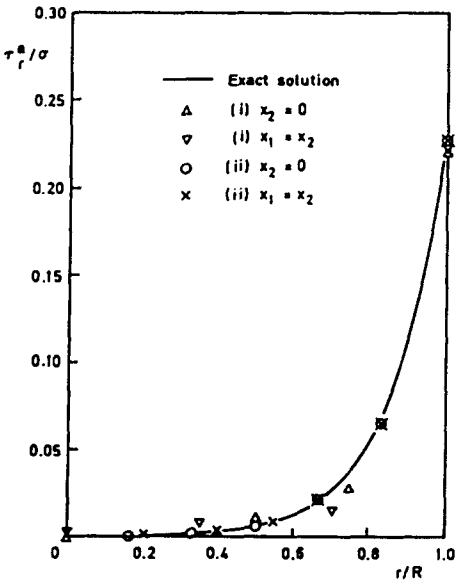

Fig. 2. Comparison of results from the boundary element model with an exact solution for a circular patch bonded to a large biaxially loaded sheet (Example 1).

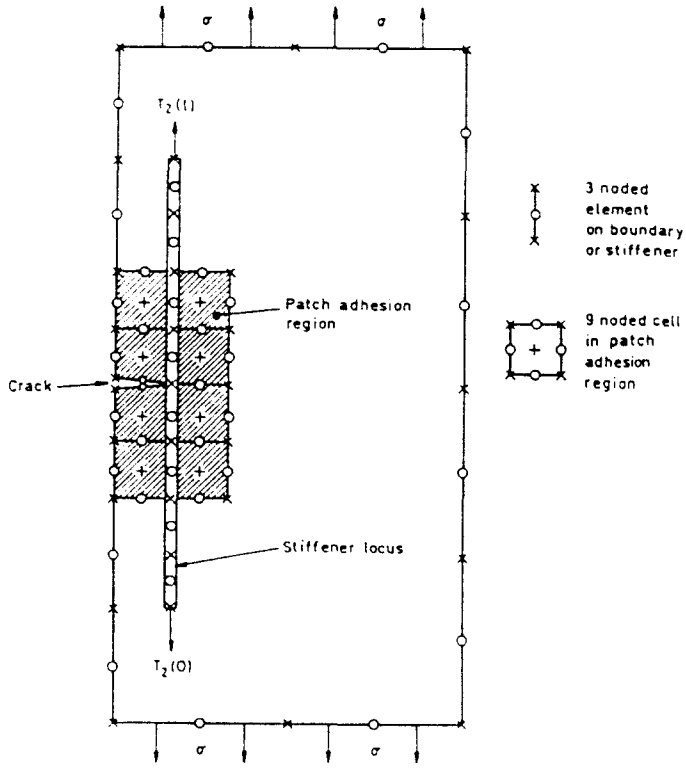

Fig. 3. Configuration of patched, stiffened edge-cracked panel showing subdivisions of boundaries, stiffener locus and patch adhesion region into elements. (Example 2 with crack length $a = 14.99$ mm.)

$E^{st} = 70$ GPa, shear modulus $G^{st} = 27$ GPa, transverse flexural rigidity $D^{st} = 175$ GPa mm^{-4}, bond line width $w^{st} = 3$ mm, adhesive layer thickness $h^{b} = 0.15$ mm and adhesive shear modulus $\mu^{b} = 0.6$ GPa. The ends of the stiffener $y = 0$ and $y = 120$ mm (corresponding to $x_2 = -60$ mm and $x_2 = 60$ mm respectively) are loaded with $T_2(0) = T_2(\ell^{st}) = \sigma B^{st} E^{st}/E^{s}$, so that locally the ends automatically deform with the sheet and the stiffener behaves as if it were much longer.

An uncracked rectangular patch of width 30 mm and height 60 mm is bonded to the sheet over the region A $\{0 \leqslant x_1 \leqslant 30$ mm, -30 mm $\leqslant x_2 \leqslant 30$ mm$\}$. It is assumed that the patch and the stiffener do not interact directly.

The boundaries and attachment regions are subdivided into elements and cells as follows. The boundary of the sheet Γ^{s} is subdivided into $8N$ elements (involving $16N+1$ nodes), the boundary of the patch Γ^{p} into $6N$ elements (with $12N$ nodes), the stiffener locus L into $4N$ elements (with $8N+1$ nodes for $a = 14.99$ mm and $8N+2$ nodes for $a = 29.99$ mm) and the adhesion region A into $2N^2$ quadratic isoparametric cells (with $(2N+1)(4N+1)+N$ nodes for $a = 14.99$ mm and $(2N+1)(4N+1)+2N$ nodes for $a = 29.99$ mm). In order to study the convergence of the results, four different meshes are considered, corresponding to $N = 2$, 4, 6 and 8. The configuration and the mesh for $N = 2$ are illustrated in Fig. 3. Note that the boundary Γ^{s} starts and ends at opposite sides of the crack and that different numbers of nodes are required on L or A for the two different crack lengths. The precise positions of the nodes common to the region A and any of Γ^{s}, Γ^{p} or L are chosen to satisfy considerations (a) and (b) in Section 5.

Various combinations of patch and stiffener are considered and Table 1 shows the values of normalized stress intensity factor $K_1/(\sigma\sqrt{\pi a})$ denoted by K^{u} for the unpatched and unstiffened sheet, K^{st} for the unpatched and stiffened sheet, K^{p} for the patched and unstiffened sheet and K^{pst} for the patched and stiffened sheet. The values of K^{u} have already converged using the crudest mesh $N = 2$ and agree with independent results (Rooke and Cartwright, 1976). The solutions for the reinforced sheets have converged satisfactorily by

Table 1. Normalized stress intensity factors $K_i/(\sigma\sqrt{\pi a})$ for patched and stiffened panels using various meshes characterized by the number N

a	N	K^u	K^{st}	K^p	K^{pst}
14.99 mm	2	1.296	1.090	0.228	0.235
	4	1.297	1.049	0.212	0.214
	6	1.297	1.033	0.208	0.208
	8	1.297	1.025	0.207	0.205
29.99 mm	2	1.788	0.827	0.204	0.206
	4	1.790	0.834	0.192	0.196
	6	1.790	0.835	0.189	0.192
	8	1.791	0.835	0.188	0.191

$N = 6$, with the largest difference between the cases $N = 6$ and $N = 8$ amounting to 0.6% for K^{pst} when $a = 14.99$ mm.

The relationships between various reinforcing effects are shown in Table 2. The reinforcing effect of the patch and the stiffener is demonstrated by the ratio of the stress intensity factors for the reinforced structure to that of the unreinforced structure. When the cracked sheet is reinforced by a patch only, this ratio is K^p/K^u. If a stiffener is present and loaded at its ends in order to simulate a section of a much larger structure, the stress intensity factor of the corresponding unreinforced sheet due to the total loading is $K^{u^*} = (1 + B^{st}E^{st}/h_sW^sE^s)K^u$ where $W^s = 90$ mm is the width of the sheet. The ratios K^{st}/K^{u^*} and K^{pst}/K^{u^*} are shown. It can be seen that the presence of the stiffener alone considerably reduces the stress intensity factor for both crack lengths, but it has much less effect when the sheet is patched ($K^p/K^u \approx K^{pst}/K^{u^*}$ to within 6%).

7. CONCLUSIONS

(1) The Boundary Element Method has been used to model a thin, cracked, finite sheet reinforced by bonded patches and stiffeners. It is assumed that the reinforced structure undergoes plane deformation only.

(2) The geometry of the configurations which may be studied is limited to cases where the crack can be described by a single straight line. The boundaries of the sheet and the patch may be arbitrarily specified and edge-cracks may be considered.

(3) The fundamental solution used in the boundary integral equations for the sheet avoids the need to satisfy boundary conditions on the crack surface and leads to exact modelling of the crack-tip singularities.

(4) Solutions are obtained numerically by subdividing the domains of integration into quadratic isoparametric elements, giving a system of simultaneous linear equations in terms of nodal values of traction and displacement on the boundaries and attachment force over the reinforced regions. Values of stress at internal points and the stress intensity factors of the crack are subsequently calculated numerically from integral formulae.

(5) Comparison of results with known solutions indicates that the model may be used to accurately analyse reinforced sheets, provided that a sufficient number of adhesion cells is used. Values of stress intensity factor converge rapidly as the mesh of boundary elements and adhesion cells is refined.

Table 2. The effect of a patch and a stiffener on the stress intensity factor for an edge cracked sheet

a	K^{st}/K^{u^*}	K^p/K^u	K^{pst}/K^{u^*}
14.99 mm	0.757	0.160	0.151
29.99 mm	0.446	0.105	0.102

REFERENCES

Abramowitz, M. and Stegun, I. (Eds) (1972). *Handbook of Mathematical Functions*. Dover, New York.

Anderson, D. G. (1965). Gaussian quadrature formulae for $\int_0^1 -\ln(x) f(x)\,dx$. *Math. Comp.* **19**, 477–481.

Bannerjee, P. K. and Butterfield, R. (1981). *Boundary Element Methods in Engineering Science*. McGraw-Hill, London.

Dowrick, G. (1987). Stress intensity factors for cracks in patched and orthogonally stiffened sheets. Ph.D. Thesis, Southampton University, U.K.

Dowrick, G., Cartwright, D. J. and Rooke, D. P. (1980). The effects of repair patches on the stress distribution in a cracked sheet. *Proc. 2nd Int. Conf. Numerical Methods in Fracture Mechanics* (Edited by D. R. J. Owen and A. R. Luxmoore), Swansea, U.K.

Erdogan, F. (1962). On the stress distribution in plates with collinear cuts under arbitrary loads. *Proc. 4th U.S. Nat. Cong. on Applied Mechanics*.

Leipholz, H. (1974). *Theory of Elasticity*. Noordhoff, Leyden.

Muskhelishvili, N. I. (1963). *Some Basic Problems on the Mathematical Theory of Elasticity*. Noordhoff, Groningen.

Rooke, D. P. and Cartwright, D. J. (1976). *Compendium of Stress Intensity Factors*. HMSO, London.

Young, A. (1988). Analysis of bonded repair patches on cracked thin sheets. Ph.D. Thesis, Southampton University, U.K.

Young, A., Cartwright, D. J. and Rooke, D. P. (1984). Influence of tapering on the stresses in repair patches. *Proc. 3rd Int. Conf. on Numerical Methods in Fracture Mechanics* (Edited by A. R. Luxmoore and D. R. J. Owen), Swansea, U.K.

Young, A., Cartwright, D. J. and Rooke, D. P. (1988). The boundary element method for analysing repair patches on cracked finite sheets. *Aero. Jl* **92**, 416–421.

Young, A., Rooke, D. P. and Cartwright, D. J. (1989). Numerical study of balanced patch repairs to cracked sheets. *Aero. Jl* **93**, 327–334.

APPENDIX

The functions $U_{ji}(\mathbf{x}, \mathbf{x}_0)$, $Y_{ji}(\mathbf{x}, \mathbf{x}_0)$, $G_{kji}(\mathbf{x}, \mathbf{x}_0)$, $Z_{kji}(\mathbf{x}, \mathbf{x}_0)$, $G^*_{kji}(\mathbf{x}, \pm a)$ and $Z^*_{kji}(\mathbf{x}, \pm a)$ for an isotropic material of Poisson's ratio ν and tensile modulus E are given below. Define $\kappa = (3-\nu)/(1+\nu)$, $\mu = \frac{1}{2}E/(1+\nu)$ and the complex variables

$$z = x_1 + ix_2, \quad z_0 = x_{01} + ix_{02}, \tag{A1}$$

corresponding to the points $\mathbf{x}$ and $\mathbf{x}_0$ respectively, where $i^2 = -1$. The complex parameter S_j $(j = 1, 2)$ is defined by

$$S_j = \frac{1}{2\pi(1+\kappa)}(\delta_{1j} + i\delta_{2j}) \tag{A2}$$

and represents the vector force $(j = 1, 2)$ per unit thickness in the fundamental solutions. A superimposed bar will be used to denote complex conjugation (e.g. $\bar{z} = x_1 - ix_2$).

The functions U_{ji} and Y_{ji} are of the form

$$U_{j1} + iU_{j2} = \frac{1}{2\mu} D_j(z, \bar{z}; z_0, \bar{z}_0), \quad Y_{j1} + iY_{j2} = -i\{(1+\kappa)\Omega_j(z; z_0, \bar{z}_0) - D_j(z, \bar{z}; z_0, \bar{z}_0)\}. \tag{A3}$$

In the Kelvin solution, Ω_j and D_j are given by

$$\Omega_j^r(z; z_0) = -S_j \log(z - z_0), \quad D_j^r(z, \bar{z}; z_0, \bar{z}_0) = -\kappa S_j \log|z - z_0|^2 + \bar{S}_j\left(\frac{z - z_0}{\bar{z} - \bar{z}_0}\right). \tag{A4}$$

It should be noted that Ω_j^r includes the complex logarithm which is a multi-valued function. When integrating over an element, $\log(z - z_0)$ must be made to vary continuously. The fundamental solution for a crack situated at $\{-a \leqslant x_1 \leqslant a, x_2 = 0\}$ involves terms Ω_j and D_j given by

$$\begin{aligned} \Omega_j(z; z_0, \bar{z}_0) &= \Omega_j^r(z; z_0) + \Omega_j^c(z; z_0, \bar{z}_0), \\ D_j(z, \bar{z}; z_0, \bar{z}_0) &= D_j^r(z, \bar{z}; z_0, \bar{z}_0) + \kappa\Omega_j^c(z; z_0, \bar{z}_0) - \Omega_j^c(\bar{z}; z_0, \bar{z}_0) - (z - \bar{z})\overline{\Omega_j^{c\prime}(z; z_0, \bar{z}_0)} \end{aligned} \tag{A5}$$

where

$$\begin{aligned} \Omega_j^c(z, z_0, \bar{z}_0) &= -\tfrac{1}{2}S_j[\kappa N_1(z, \bar{z}_0) - N_1(z, z_0)] - \tfrac{1}{2}\bar{S}_j(\bar{z}_0 - z_0)N_2(z, \bar{z}_0) \\ \Omega_j^{c\prime}(z; z_0, \bar{z}_0) &= \frac{\partial}{\partial z}\Omega_j(z; z_0, \bar{z}_0) \\ &= -\tfrac{1}{2}(z^2 - a^2)^{-1/2}\{S_j[\kappa M_1(z, \bar{z}_0) - M_1(z, z_0)] + \bar{S}_j(\bar{z}_0 - z_0)M_2(z, \bar{z}_0)\} \end{aligned} \tag{A6}$$

$$N_1(z,z_0)=\log\left[\frac{2(zz_0-a^2+(z^2-a^2)^{1/2}(z_0^2-a^2)^{1/2})}{(z+(z^2-a^2)^{1/2})(z_0+(z_0^2-a^2)^{1/2})}\right]$$

$$N_2(z,z_0)=(z_0^2-a^2)^{-1/2}M_1(z,z_0)$$

$$M_1(z,z_0)=\frac{(z^2-a^2)^{1/2}-(z_0^2-a^2)^{1/2}}{z-z_0}-1$$

$$M_2(z,z_0)=[M_1(z,z_0)+1-z_0(z_0^2-a^2)^{-1/2}]/(z-z_0) \tag{A7}$$

and the complex square root function $(z^2-a^2)^{1/2}$ is defined to be the continuous branch for which $\lim_{z\to\infty}\{(z^2-a^2)^{1/2}/z\}=1$.

The functions G_{kj} and Z_{kj} are of the form

$$G_{1j1}+iG_{1j2}=\frac{1}{2\mu}\left(\frac{\partial}{\partial z_0}+\frac{\partial}{\partial\bar z_0}\right)D_j(z,\bar z;z_0,\bar z_0)$$

$$G_{2j1}+iG_{2j2}=\frac{i}{2\mu}\left(\frac{\partial}{\partial z_0}-\frac{\partial}{\partial\bar z_0}\right)D_j(z,\bar z;z_0,\bar z_0)$$

$$Z_{1j1}+iZ_{1j2}=-i\left\{(1+\kappa)\left(\frac{\partial}{\partial z_0}+\frac{\partial}{\partial\bar z_0}\right)\Omega_j(z;z_0,\bar z_0)-2\mu(G_{1j1}+iG_{1j2})\right\}$$

$$Z_{2j1}+iZ_{2j2}=-i\left\{(1+\kappa)i\left(\frac{\partial}{\partial z_0}-\frac{\partial}{\partial\bar z_0}\right)\Omega_j(z;z_0,\bar z_0)-2\mu(G_{2j1}+iG_{2j2})\right\} \tag{A8}$$

and the derivatives from the two fundamental solutions (A4) and (A5) are given by

$$\frac{\partial D_j^c}{\partial z_0}=\frac{\kappa S_j}{z-z_0}-\frac{\bar S_j}{\bar z-\bar z_0},\quad \frac{\partial D_j^c}{\partial\bar z_0}=\frac{\kappa S_j}{\bar z-\bar z_0}+\frac{\bar S_j(z-z_0)}{(\bar z-\bar z_0)^2},\quad \frac{\partial\Omega_j^c}{\partial z_0}=\frac{S_j}{z-z_0},\quad \frac{\partial\Omega_j^c}{\partial\bar z_0}=0,$$

$$\frac{\partial D_j^r}{\partial z_0}=\kappa\Psi_1(z;z_0,\bar z_0)-\Psi_1(\bar z;z_0,\bar z_0)-(z-\bar z)\overline{\Psi_2(z;z_0,\bar z_0)},$$

$$\frac{\partial D_j^r}{\partial\bar z_0}=k\Psi_1(z;z_0,\bar z_0)-\Psi_1(\bar z;z_0,\bar z_0)-(z-\bar z)\overline{\Psi_4(z;z_0,\bar z_0)},$$

$$\frac{\partial\Omega_j^r}{\partial z_0}=\Psi_1(z;z_0,\bar z_0),\quad \frac{\partial\Omega_j^r}{\partial\bar z_0}=\Psi_1(z;z_0,\bar z_0), \tag{A9}$$

where

$$\Psi_1(z;z_0,\bar z_0)=\tfrac12\{S_jQ_1(z,z_0)+\bar S_j(N_2(z,\bar z_0)\}$$

$$\Psi_2(z;z_0,\bar z_0)=\tfrac12(z^2-a^2)^{-1/2}\{S_jM_2(z,z_0)+\bar S_jM_2(z,\bar z_0)\}$$

$$\Psi_3(z;z_0,\bar z_0)=-\tfrac12\{\kappa S_jQ_1(z,\bar z_0)+\bar S_j[N_2(z,\bar z_0)+(\bar z_0-z_0)Q_2(z,\bar z_0)]\}$$

$$\Psi_4(z;z_0,\bar z_0)=-\tfrac12(z^2-a^2)^{-1/2}\{\kappa S_jM_2(z,\bar z_0)+\bar S_j[M_2(z,\bar z_0)+(\bar z_0-z_0)P_2(z,\bar z_0)]\} \tag{A10}$$

$$P_2(z,z_0)=[2M_2(z,z_0)+a^2(z_0^2-a^2)^{-3/2}]/(z-z_0)$$

$$Q_1(z,z_0)=(z_0^2-a^2)^{-1/2}M_1(z,z_0)$$

$$Q_2(z,z_0)=\{M_2(z,z_0)-z_0(z_0^2-a^2)^{-1}[M_1(z,z_0)+1]\}/(z_0^2-a^2)^{1/2}. \tag{A11}$$

The singular terms $(1/\rho)\Phi_{kj}(\varphi)$ defined in eqn (49), where $z-z_0=\rho e^{i\varphi}$, are of the form

$$\Phi_{1j1}+i\Phi_{1j2}=\frac{1}{2\mu}[A_j(\varphi)+B_j(\varphi)]\quad \Phi_{2j1}+i\Phi_{2j2}=\frac{i}{2\mu}[A_j(\varphi)-B_j(\varphi)]. \tag{A12}$$

For the Kelvin solution, $A_j(\varphi)$ and $B_j(\varphi)$ are given by

$$A_j^K(\varphi)=\kappa S_je^{-i\varphi}-\bar S_je^{i\varphi}\quad B_j^K(\varphi)=\kappa S_je^{i\varphi}+\bar S_je^{3i\varphi} \tag{A13}$$

and for the cracked sheet solution, $A(\varphi)$ and $B(\varphi)$ are given by

$$A_j(\varphi)=A_j^K(\varphi)-\kappa\bar S_j(e^{i\varphi}+e^{-3i\varphi})+(S_j+\kappa\bar S_j)e^{3i\varphi}\quad B_j(\varphi)=B_j^K(\varphi)+S_j(e^{i\varphi}-e^{3i\varphi})+(\kappa^2S_j+\kappa\bar S_j)e^{-i\varphi}. \tag{A14}$$

The kernels $G^*_{kj}(x,\pm a)$ and $Z^*_{kj}(x,\pm a)$ required to calculate the stress intensity factors in eqn (15) are related to four functions $\Psi^*_n(z,\pm a)$ $(n=1,2,3,4)$ in the same way that the stress kernels $G_{kj}(x,x_0)$ and $Z_{kj}(x,x_0)$ involve the four functions $\Psi_n(z;z_0,\bar z_0)$ $(n=1,2,3,4)$ in eqns (A9)–(A11). The terms Ψ^*_n are of the form

$$\Psi^*_1(z,\pm a)=-\frac12\left(\frac{\pi}{a}\right)^{1/2}(S_j+\bar S_j)\psi(z,\pm a)\quad \Psi^*_2(z,\pm a)=-\frac12\left(\frac{\pi}{a}\right)^{1/2}(S_j+\bar S_j)\psi'(z,\pm a)$$

$$\Psi^*_3(z,\pm a)=\frac12\left(\frac{\pi}{a}\right)^{1/2}(\kappa\bar S_j+S_j)\psi(z,\pm a)\quad \Psi^*_4(z,\pm a)=\frac12\left(\frac{\pi}{a}\right)^{1/2}(\kappa\bar S_j+S_j)\psi'(z,\pm a) \tag{A15}$$

where

$$\psi(z, \pm a) = \left(\frac{z \pm a}{z \mp a}\right)^{1/2} - 1 \quad \psi'(z, \pm a) = \frac{\mp a}{(z \mp a)(z^2 - a^2)^{1/2}}. \tag{A16}$$

Finally, the second integral in eqn (18) is given by

$$\int_{-1}^{+1}\int_{-1}^{+1} \log[(\gamma_1 - \gamma_{01})^2 + (\gamma_2 - \gamma_{02})^2]\, d\gamma_1\, d\gamma_2 = [g(1-\gamma_{01}, 1-\gamma_{02}) + g(1+\gamma_{01}, 1+\gamma_{02}) - g(1-\gamma_{01}, 1+\gamma_{02}) - g(1+\gamma_{01}, 1-\gamma_{02})] \tag{A17}$$

where

$$g(\alpha, \beta) = \alpha\beta \log(\alpha^2 + \beta^2) - 3\alpha\beta + \alpha^2 \tan^{-1}(\beta/\alpha) + \beta^2 \tan^{-1}(\alpha/\beta). \tag{A18}$$